EAI Endorsed Transactions
on Sustainable Manufacturing and Renewable Energy Research Article EAI.EU

Robust Hybrid LQR - Integral Control for 2-DOF Robotic Arms: Performance Evaluation under Simulated Agricultural Vibration Conditions

N. L. Quang [1,2]

[1]Department of Mechatronic Engineering, Faculty of Mechanical Engineering, Ho Chi Minh city University of Technology (HCMUT), 268 Ly Thuong Kiet, Dien Hong Ward, Ho Chi Minh City, Vietnam.
[2]Vietnam National University Ho Chi Minh city, Linh Trung Ward, Ho Chi Minh City, Vietnam.

Abstract

Robotic technologies, particularly robotic manipulators, play an important role in both industrial automation and smart agriculture. In agricultural sectors where automation remains underutilized and labor cost is high, robotic solutions are necessary for enhancing productivity. However, developing agricultural robots faces significant challenges due to harsh environmental conditions, limited resources, and strict human-robot collaboration safety requirements. Consequently, advanced control algorithms are critical for maintaining high precision under operational disturbances, such as vibrations from internal combustion engine-powered tractors. This study proposes a robust Linear-Quadratic Regulator combined with Integral control (LQR-KI) for 2-DOF flexible joint robots. While flexible joint manipulators offer a safety and reduced structural weight compared to traditional rigid systems, they are affected by complex, non-ideal coupling vibrations. The proposed control structure focuses on enhancing stability and positioning accuracy, with its robustness verified through an extensive analysis of closed-loop pole trajectories under non-ideal agricultural excitations. Numerical simulations demonstrate that the LQR - KI scheme effectively isolates base vibrations, achieving a significant link positioning accuracy of 0.03 (rad). Especially, the results validate that the flexible joint configuration, optimized by the proposed controller, can achieves approximately **9.36%** energy savings compared to conventional rigid-link counterparts. This research contributes to sustainable production by providing a high-performance, energy-efficient solution for integrating advanced robots into existing agricultural platforms.

Keywords: Non-ideal source; LQR control; Robotic manipulators; Smart agriculture; Sustainable agriculture; Energy efficiency.

Received on 07 December 2025, accepted on 03 February 2026, published on 05 February 2026

Copyright © 2026 N.L. Quang, licensed to EAI. This is an open access article distributed under the terms of the CC BY-NC-SA 4.0, which permits copying, redistributing, remixing, transformation, and building upon the material in any medium so long as the original work is properly cited.

doi: 10.4108/eetsmre.11257

1. Introduction

Robotic systems have become a foundational element of modern industrial automation, driven by trends such as Industry 4.0 and the increasing demand for high-speed, flexible, and production processes that involve people directly [22]. Robotic arms are moving away from heavy-duty, stiff-joint configurations toward lighter, more flexible designs, supporting safe human-robot interaction and efficient operation [23]. Among these designs, manipulators equipped with flexible joints stand out due to their reduced inertia, simplified mechanical structure, and enhanced dynamic performance. Therefore, they allow for safer operation in shared human environments and contribute to faster repositioning in repetitive tasks.

We assume that these flexible-joint designs are uniquely suited for smart agriculture, where joint elasticity serves as

a vital feature for safe interaction with human workers and delicate crops. In this context, collaborative robots (cobots) are increasingly necessary for precision tasks like harvesting and spraying. However, integrating elasticity introduces significant technical challenges, such as complex coupling vibrations and difficulties in trajectory tracking [24, 25]. While recent work has explored smart control methods, adaptive algorithms, and vibration suppression strategies [6], many of these solutions incur high computational costs, require extensive modeling or tuning, and may be difficult to implement in practical agricultural field environments.

Beyond the nonlinear control research mentioned above, considering linear control methods for these models is essential, especially under constraints of limited power, memory resources, and harsh environmental conditions typical of agricultural settings. Tusset et al proposed a hybrid controller combining concepts of a PID controller with LQR and a feedforward gain to control the positioning of 2-DOF flexible-joint robotic arm operating under non-ideal excitations [1, 27]. Positioned within the specific context of robotic applications in smart farming, this study proposes a robust Linear-Quadratic Regulator combined with Integral control (LQR-KI) for a 2-DOF flexible-joint robotic arm operating under non-ideal agricultural excitations. By replacing complex feedforward terms with a simplified integral action, we aim to achieve an optimal balance between implementation simplicity and superior vibration suppression, while significantly improving energy efficiency by approximately 9.36%.

2. Literature Review

Classical control strategies such as PID and model-based feedback have been widely used for robotic manipulators [2,3,14]. These approaches are relatively simple to implement and tune, and they are still the dominant choice in many industrial applications. However, when joint flexibility, parameter uncertainties or fast trajectories are involved, purely PID-based designs may suffer from poor transient performance and limited robustness.

In the case of flexible or flexible-joint manipulators, the control problem becomes more challenging due to elastic deformation, vibration propagation and strong coupling between links [2,4,5]. Various strategies have been proposed to control these effects, including intelligent control [4], adaptive prescribed performance control [5], model predictive control [8]. While these nonlinear methods achieve high precision in laboratory settings, they often require high-end processing units, making them less ideal for harsh agricultural environments where energy efficiency and hardware cost-effectiveness are necessary.

Robust and adaptive control scenarios have also been studied to face disturbances, unknown parameters and non-ideal excitations [6,11,13,15,16,17,21]. These aim to guarantee performance but often at the cost of increased implementation complexity and heavy computational processes. In agricultural cobots, there is a clear necessity for controllers that balance simplicity with effective vibration suppression.

A different direction focuses on combining classical structures with optimal techniques like LQR to achive the advantages of both. Tusset et al. investigated a hybrid scheme for manipulators under non-ideal excitation, providing a foundation for improvements in position control. Inspired by these results, this paper proposes an LQR-KI strategy applied to an 8th-order linear state-space model. Our goal is to ensure the controller is mathematically rigorous yet light enough for standard microcontrollers, while demonstrating that optimized flexible joints can achieve approximately 9.36% energy savings over rigid counterparts.

3. Methodology

3.1 The dynamic model

The mechanical system diagram of the robotic arm with flexible joint can be shown in Fig. 1 where the angular coordinates are $\boldsymbol{\theta} = [\theta_1\ \theta_2]^T$ and $\boldsymbol{\theta_M} = [\theta_3\ \theta_4]^T$ the rectangular coordinates $p_1 = [p_{1x}\ p_{1y}]$, $p_2 = [p_{2x}\ p_{2y}]$. The system consists of two rigid links $L_1 and\ L_2$, connected through two flexible joints characterized by the joint stiffness k_b. The second link is excited by a DC motor.

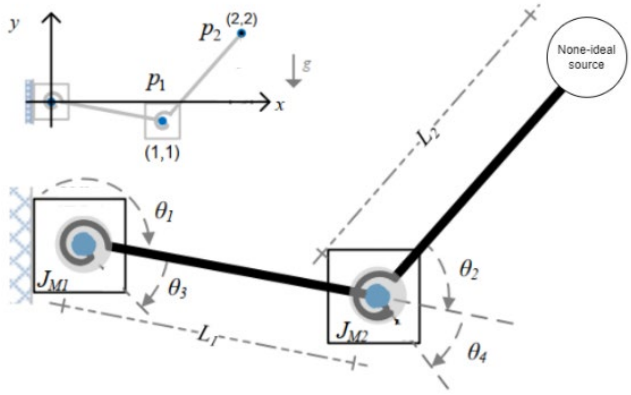

Fig. 1. Schematic of 2 DoFs Robot arm

As figure 1, the dynamic model of the robotic manipulator can be divided into two components: the link positions $(\boldsymbol{\theta})$ – link side and the motor positions $(\boldsymbol{\theta_M})$ - motor side

The link-side are derived using the Euler–Lagrange formulation, resulting in the following equations **[1,27]:**

$$\boldsymbol{M(\theta)(\ddot{\theta}) + V(\theta,\dot{\theta})\dot{\theta} + G(\theta) + F_a\dot{\theta} = T_{flexible}} \quad \textbf{(1)}$$

Here: M is the matrix of inertia, V is the matrix of Coriolis and centrifugal force, G is the gravity vector, F_a is the vector of viscous and $T_{flexible}$ is the applied torque.

$$\boldsymbol{M} = \begin{bmatrix} \boldsymbol{m_{11}} & \boldsymbol{m_{12}} \\ \boldsymbol{m_{21}} & \boldsymbol{m_{22}} \end{bmatrix}, \boldsymbol{V} = \begin{bmatrix} \boldsymbol{V_1} \\ \boldsymbol{V_2} \end{bmatrix}, \boldsymbol{G} = \begin{bmatrix} \boldsymbol{g_{11}} \\ \boldsymbol{g_{22}} \end{bmatrix}, \boldsymbol{F_a} = \begin{bmatrix} \boldsymbol{k_a} \\ \boldsymbol{k_a} \end{bmatrix}$$

$$\boldsymbol{T_{flexible}} = \begin{bmatrix} \boldsymbol{b_s}(\dot{\boldsymbol{\theta}}_3 - \dot{\boldsymbol{\theta}}_1) + \boldsymbol{k_b}(\boldsymbol{\theta_3} - \boldsymbol{\theta_1}) \\ \boldsymbol{b_s}(\dot{\boldsymbol{\theta}}_4 - \dot{\boldsymbol{\theta}}_2) + \boldsymbol{k_b}(\boldsymbol{\theta_4} - \boldsymbol{\theta_2}) \end{bmatrix}.$$

Where b_s is joint damping coefficient, k_b is the stiffness ratio of spring, k_a link viscous friction coefficient. In this case, for simplicity in control design, the moment of inertia of the links about their center of mass I_1, I_2 are assumed to be zero, effectively treating the links as point masses located at their center of gravity $l_{ci}, (i = 1,2)$.

$m_{11} = m_1 l_{c1}^2 + m_2 l_1^2 + m_2 l_{c2}^2 + 2m_2 l_1 l_{c2} \cos(\theta_2)$;
$m_{21} = m_{12} = m_2 l_{c2}^2 + l_1 l_2 m_2 \cos(\theta_2)$;
$and\ m_{22} = l_{c2}^2 m_2$.
$v_{11} = -m_2 l_1 l_{c2} \sin(\theta_2)\dot{\theta}_2 + 2\dot{\theta}_1\dot{\theta}_2$;
$v_{22} = m_2 l_1 l_{c2} \sin(\dot{\theta}_2)(2\dot{\theta}_1 + \dot{\theta}_2)$;
$g_{11} = (ml_{c1} + m_2 l_1) g \sin(\theta_1) - m_2 g l_{c2} \sin(\theta_1 + \theta_2)$;
$g_{22} = m_2 g l_{c2} \sin(\theta_1 + \theta_2)$;

The motor-side dynamics ($\theta_3\ and\ \theta_4$) of the flexible-joint robot are aslo derived using the Euler–Lagrange formulation, resulting in the following equations [1,27]:

$$\boldsymbol{J\ddot{\theta}_m + B_v\theta_m = \tau_m - T_{flexible}} \qquad \textbf{(2)}$$

Where **J** is presented the motor-side inertia, $\boldsymbol{b_v}$ is the rotor damping coefficient**,** $\boldsymbol{k_t}$ represents the motor torque constant, and $\boldsymbol{i}$ is the DC motor current.

After establishing the mathematical model, we will conduct a linearization the system around the equilibrium point: $\boldsymbol{x_0} = [\boldsymbol{\theta_{1d}}, \boldsymbol{0}, \boldsymbol{\theta_{2d}}, \boldsymbol{0}, \boldsymbol{\theta_{1d}}, \boldsymbol{0}, \boldsymbol{\theta_{2d}}, \boldsymbol{0}]^{\boldsymbol{T}}$, with the equation:

$$\boldsymbol{\dot{x} = Ax + Bu} \qquad \textbf{(3)}$$

To facilitate the design of the linear optimal controller, the nonlinear state-space model in (4) must be linearized. In this study, instead of linearizing around a conventional zero-equilibrium, where the robot is at rest at the desire positions, we adopt a more rigorous approach by selecting a worst-case operating point. This strategy is particularly relevant for resource-constrained agricultural robotics, where the controller must remain robust under the most demanding dynamic conditions.

An additional stability survey was conducted, analyzing both gain margins (**GM**) and phase margins (**PM**) across the manipulator's workspace to identify the system's worst-case configuration $[\boldsymbol{\theta_{link1}}; \boldsymbol{\theta_{link2}}]$. This critical point, where the system exhibits its lowest stability margins, was strategically selected as the equilibrium point for Jacobian linearization. We consider five representative operating points were evaluated to determine this boundary condition:

Table 1. Evaluating worst-case point open-loop system

Operational point	GM/PM Link 1	GM/PM Link 2	Analyst's stability
[0;0]	150.32 dB/ inf	131.08 dB/ inf	stable
$[\frac{\pi}{4};\frac{\pi}{4}]$	39.86 dB/ inf	27.70 dB/ inf	stable
$[0;\frac{\pi}{2}]$	42.08 dB/ inf	36.80 dB/ 89.03 deg	stable
$[\frac{\pi}{2};0]$	150.32dB/ 65.95deg	-17.48 dB/ 87.70 deg	Unstable/ worst-case
$[\frac{\pi}{2};\frac{\pi}{2}]$	39.02 dB/ -87.27 deg	130.52 dB/ 94.73 deg	Unstable

Analysis reveals that the system exhibits instability at the configurations [π/2;0] and [π/2; π/2] due to negative gain margins. To ensure global stability under resource-constrained agricultural conditions, this study strategically selected the configuration [π/2;0] as the equilibrium point for Jacobian matrix linearization. This selection is driven by the fact that the system is most unstable at this point, particularly with a negative gain margin of -17.48 dB at the second link. Moreover, the positioning precision of Link 2 is the primary target for effective agricultural task execution, so prioritizing its stability at this critical boundary is essential.

Consider the equilibrium point:

$$\boldsymbol{x_0} = \left[\frac{\boldsymbol{\pi}}{\boldsymbol{2}}, \boldsymbol{0}, \boldsymbol{0}, \boldsymbol{0}, \frac{\boldsymbol{\pi}}{\boldsymbol{2}}, \boldsymbol{0}, \boldsymbol{0}, \boldsymbol{0}\right]^{\boldsymbol{T}}$$

. The state-space linearization equation:

$$\boldsymbol{\Delta\dot{x} = A\Delta x + B\Delta u} \qquad \textbf{(4)}$$

The state vector is defined as:

$$x^T = \begin{bmatrix} x_1 \\ x_2 \\ x_3 \\ x_4 \\ x_5 \\ x_6 \\ x_7 \\ x_8 \end{bmatrix} = \begin{bmatrix} \theta_1 \\ \dot{\theta}_1 \\ \theta_2 \\ \dot{\theta}_2 \\ \theta_3 \\ \dot{\theta}_3 \\ \theta_4 \\ \dot{\theta}_4 \end{bmatrix}; \textbf{(5)}$$

and the control input is $u = [i_1, i_2]^T$

Or more detail [1,27] the equation of system is described as below:

$$\begin{aligned} \dot{\boldsymbol{x}}_{\boldsymbol{1}} &= \boldsymbol{x_2} \\ \dot{\boldsymbol{x}}_{\boldsymbol{2}} &= -\boldsymbol{p_{11}k_b\,x_1} + \boldsymbol{\alpha x_2} - \boldsymbol{p_{12}k_b x_3} + \boldsymbol{\beta x_4} + \boldsymbol{p_{11}k_b\,x_5} + \boldsymbol{p_{11}b_s x_6} + \boldsymbol{p_{12}\,k_b x_7} + \boldsymbol{p_{12}\,b_s x_8} - \boldsymbol{p_{11}g_1} - \boldsymbol{p_{12}g_2}\,. \\ \dot{\boldsymbol{x}}_{\boldsymbol{3}} &= \boldsymbol{x_4} \\ \dot{\boldsymbol{x}}_{\boldsymbol{4}} &= -\boldsymbol{p_{21}k_b x_1} + \boldsymbol{\gamma x_2} - \boldsymbol{p_{22}k_b\,x_3} + \boldsymbol{\delta\,x_4} + \boldsymbol{p_{21}k x_5} + \boldsymbol{p_{21}b\_s x_6} + \boldsymbol{p_{22}k\,x_7} + \boldsymbol{p_{22}\,b_s\,x_8} - \boldsymbol{p_{21}\,g_1} - \boldsymbol{p_{22}g_2}. \end{aligned} \qquad \textbf{(6)}$$

$$\begin{aligned}
\dot{x_5} &= x_6 \\
\dot{x_6} &= \frac{1}{J}(-k\,x_1 + b_s\,x_2 - k\,x_5 - \\
&(b_v + b_s)x_6 + k_t\,i_1). \\
\dot{x_7} &= x_8 \\
\dot{x_8} &= \frac{1}{J}(-k\,x_3 + b_s x_4 - k\,x_7 - \\
&(b_v + b_s)x_8 + k_t\,i_2).
\end{aligned}$$

Where damping components are: $\alpha = -p_{11}(k_a + b_s) - p_{12}b_s$, $\beta = p_{11}\mathrm{b_s} - p_{12}(k_a + b_s)$, $\gamma = -p_{21}(k_a + b_s) - p_{22}\mathrm{b_s}$, $\delta = -p_{22}(k_a + b_s) + p_{21}b_s$; and components of matrix $P = M^{-1}$ are calculated as below:

$$p_{11} = \frac{m_{22}}{-m_{12}m_{21} + m_{11}m_{22}},$$
$$p_{12} = -\frac{m_{12}}{-m_{12}m_{21} + m_{11}m_{22}},$$
$$p_{21} = \frac{-m_{21}}{-m_{12}m_{21} + m_{11}m_{22}}, p_{22} = \frac{m_{11}}{-m_{12}m_{21} + m_{11}m_{22}}$$

In summary, the 8th-order dynamic model presented in this section provides a comprehensive and rigorous representation of the 2-DOF flexible-joint manipulator. By systematically deriving the link-side and motor-side equations, this work clarifies and improves upon inconsistencies regarding symbol conventions and structural matrices found in previous literature [1, 27]. Furthermore, by linearizing the system at the identified worst-case operating point, this refined model serves as a robust mathematical foundation for the development of the LQR-KI control strategy. This approach ensures that the subsequent control design remains stable and energy-efficient under the most precarious agricultural operating conditions.

3.2 Proposed Control: Robust LQR-KI

The position control of the motor links and motor shafts is implemented via the input current $U = [U_1\ U_2]^T$. The motor torque $\tau = k_t i$ introducing the control input through the motor current modifies the motor-side dynamics in (4). By replacing $i_1 = U_1\ and\ i_2 = U_2$ into the system equations **(6),** the coupled link–motor dynamics can be rewritten in the following state-space equations :

$$\begin{aligned}
\dot{x_6} &= \frac{1}{J}(-k\,x_1 + b_s\,x_2 - k\,x_5 - \\
&(b_v + b_s)x_6 + k_t\,U_1). \\
\dot{x_8} &= \frac{1}{J}(-k\,x_3 + b_s\,x_4 - k\,x_7 - \\
&(b_v + b_s)x_8 + k_t\,U_2).
\end{aligned} \quad (7)$$

This controlled state-space model serves as the foundation for the hybrid LQR–KI control strategy.

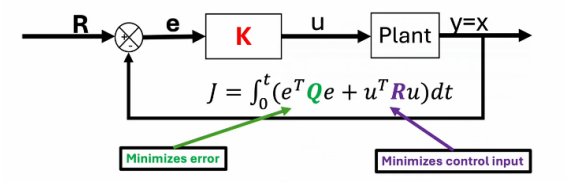

Fig. 2. LQR block diagram

In this study, a Linear Quadratic Regulator (LQR) is applied to calculate the optimal proportional and derivative gains for the 8th-order linearized state-space model. The primary objective is to design an optimal cost function, J, that balances trajectory tracking accuracy and energy consumption efficiency. The LQR framework minimizes the following cost function

$$\boldsymbol{J = \frac{1}{2}\int_{t_0}^{\infty}(e^T Qe + u^T Ru)dt} \quad \textbf{(8)}$$

Where Q and R are positive-definite weighting matrices selected to penalize state deviations and control effort, respectively. The optimal feedback gain matrix K is determined by solving the Algebraic Riccati Equation (ARE)

$$\boldsymbol{A^T P + PA - PBR^{-1}B^T P + Q = 0} \quad \textbf{(9)}$$

The resulting optimal gain matrix is computed as:

$$\boldsymbol{K = R^{-1}B^T P} \quad \textbf{(10)}$$

In this 8th-order configuration, the odd-indexed gains ($K_{1,3,5,7}$) are mapped to the proportional components, while the even-indexed gains ($K_{2,4,6,8}$) are mapped to the derivative components of the state-feedback law. This optimal tuning is a critical step before introducing the integral action, as it establishes a high-performance baseline for vibration suppression and energy-efficient positioning in agricultural tasking.

Fundamentally, the LQR design process for the 8th-order model optimizes the proportional and derivative gains, effectively functioning as an optimal PD controller where the feedback matrix K maps to the system's velocity and position states. However, a standard PD structure often fails to eliminate steady-state errors caused by gravitational torques and non-ideal agricultural disturbances without a complex feedforward compensator.

To ensure robust tracking and disturbance elimination, this study proposes an extended model derived from the 8-state variable model **(4)** with the addition of position error integral states. By augmenting the state vector to a 10th-order system, the controller can thoroughly resolve remaining offsets and autonomously compensate for non-ideal excitations. This approach contributes to creating an

optimal and consistent control architecture that maintains high precision, achieving a good positioning accuracy.

The state vector is augmented as follows:

$$x_{aug} = \begin{bmatrix} x \\ z \end{bmatrix} = [x_1, x_2, x_3, x_4, x_5, x_6, x_7, x_8, \int e_1 dt, \int e_2 dt]^T \quad (11)$$

Where $z = [z_1, z_2]^T$ represents the integral of the positioning errors for link 1 and link 2. The resulting 10th-order augmented state-space system is described by:

$$\dot{x}_{aug} = \hat{A}x_{aug} + \hat{B}u \quad (12)$$

The augmented system matrices $\hat{A}$ and $\hat{B}$ are constructed as:

$$\hat{A} = \begin{bmatrix} A & 0_{8\times2} \\ Cq & 0_{2\times2} \end{bmatrix}, \hat{B} = \begin{bmatrix} B \\ 0_{2\times2} \end{bmatrix} \quad (13)$$

In this formulation, A and B are the Jacobian matrices linearized at the worst-case operating point [π/2;0], and C_q is the output matrix that extracts the positioning errors of the links. By solving the Algebraic Riccati Equation for this augmented system, the optimal gain matrix $\hat{K} = [K_{LQR}|K_i]$ is obtained.

3.3 Stability analysis via observation of poles distribution.

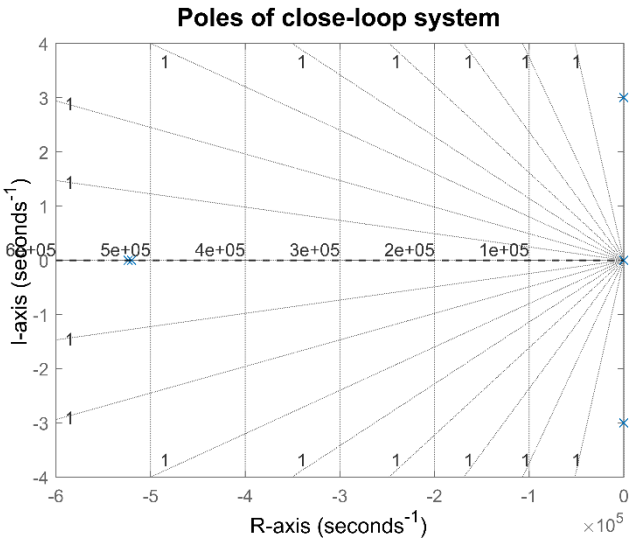

Fig. 3. Poles of close-loop system

The closed-loop pole-zero map provides a clear validation of the proposed LQR-KI controller's effectiveness. Key observations are summarized as follows:

Global Asymptotic Stability: All ten closed-loop poles are strictly located in the left-half of the complex plane, confirming that the system achieves robust stability even at the worst-case configuration [π/2;0].

Ultra-Fast Actuator Response: The presence of deep real poles at -5.2×10^{-5} demonstrates the controller's ability to react instantaneously to motor torque fluctuations and current dynamics.

Effective Vibration Damping: The complex conjugate pairs $(-2.3 \pm 3.i)$ indicates negative real components, indicating that the LQR-KI scheme effectively suppresses elastic oscillations from the flexible joints ($k_b = 400, b_s = 520$).

Integral Action Efficiency: The dominant poles near the imaginary axis confirm that the integral action (K_I) eliminates steady-state errors without inducing excessive overshoot or undesirable oscillations.

In conclusion, these results show a promising and reliable foundation for a robust control structure, that the proposed LQR-KI controller provides the stability to the harsh and unpredictable disturbances in agricultural environments. This mathematical validation provides a high level of confidence in the controller's ability to maintain precision and operational integrity under extreme field conditions.

4. Numerical Simulation

The following parameters are used for the numerical simulations:$m_1 = m_2 = 10, l_1 = l_2 = 0.8, g = 9.81, k_b = 400, b_s = 520, k_a = 5, b_v = 0.02, J = 0.02, k_t = 0.8$. The initial conditions $x_{1,..,8}(0) = 0$.

Three simulation scenarios are considered to evaluate the performance of the proposed controller. In the first scenario, both links are positioned at fixed reference points. In the second scenario, the first link and second link are moving under disturbance. In the third scenario, this study conducts a validation to compare the energy consumption between flexible joint and rigid-joint under disturbance excitation.

The weighting matrices Q and R used in the LQR design, together with the system matrices A and B, are provided in the appendix.

4.1 Position Control for Fixed Points

In the first simulation scenario, both links are commanded to reach fixed reference points under ideal conditions to evaluate steady-state accuracy.

Considering the desired states $\tilde{x}_1 = \tilde{x}_5 = \frac{\pi}{2}; \tilde{x}_3 = \tilde{x}_7 = \frac{\pi}{4}; \tilde{x}_2 = \tilde{x}_4 = \tilde{x}_6 = \tilde{x}_8 = 0$.

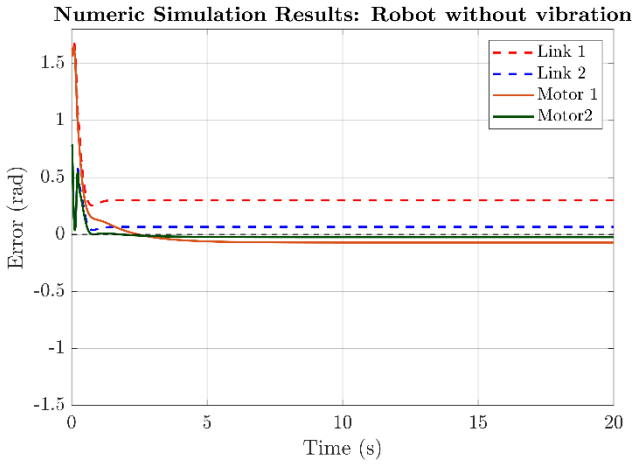

Fig. 4. Positioning error for LQR control; for error for $\theta_1, \theta_2, \theta_3, \theta_4$,

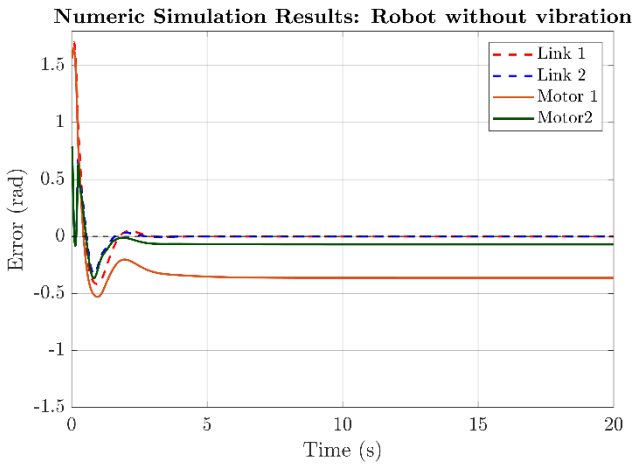

Fig. 5. Positioning error for LQR control with KI control; for error for $\theta_1, \theta_2, \theta_3, \theta_4$.

To evaluate the system's response in greater detail, a comparative analysis was conducted using the Root Mean Square Error **(RMSE)** metric.

Table 2. RMSE in case without vibration excitation

Ele-ments	K_LQR	K_LQR+KI
Link 1	0.299984	0.000000
Link 2	0.066242	0.000000
Motor 1	0.070402	0.363295
Motor 2	0.023273	0.069296

LQR Control (PD-based): As illustrated in **Fig. 4**, the standard LQR controller (functioning as an optimal PD regulator) fails to eliminate the steady-state error, particularly for the links. Due to the uncompensated gravitational torques and joint elasticity, link 1 exhibits a significant residual offset with an RMSE of approximately ~0.3 rad.

LQR-KI Control (Proposed): In contrast, **Fig. 5** demonstrates that the proposed LQR-KI controller effectively drives the positioning errors of both Link 1 and Link 2 to zero (0.000000 RMSE).

Conclusion: The addition of the integral states successfully solves the problem for the non-linear gravitational effects without requiring a complex feedforward model. [1, 27].

4.2 Position Control under vibration disturbance

In this case, we consider the desired condition: $\tilde{x}_1 = \tilde{x}_5 = \frac{\pi}{2}, \tilde{x}_3 = \tilde{x}_7 = \frac{\pi}{4}$, with a non-ideal source excitation to the link 1. A source Z=0.01sin100t is added to θ_{link1} as disturbance from displacement, z = 0.01cost is added to $\dot{\theta}_{link1}$ from velocity. This is seen as the system is subjected to non-ideal vibrations to simulate harsh agricultural field conditions. A rotational motion representing an unbalanced motor mass is injected as a disturbance to evaluate the robustness of the control strategies

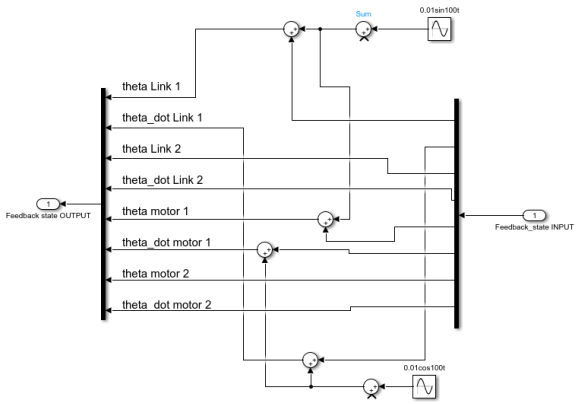

Fig. 6 Disturbance input to link and motor 1

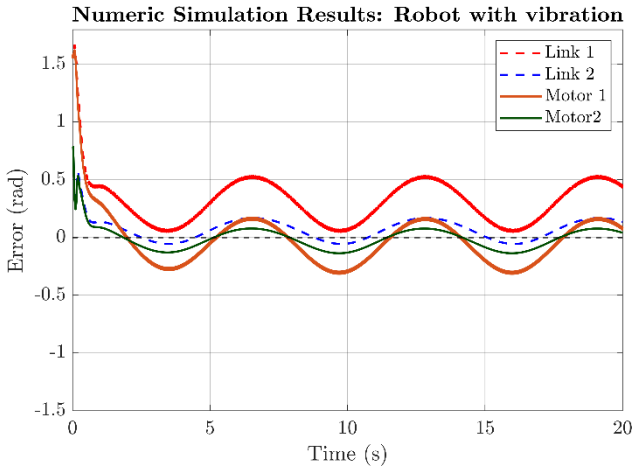

Fig. 7. Positioning error for LQR control for error for $\theta_1, \theta_2, \theta_3, \theta_4,$

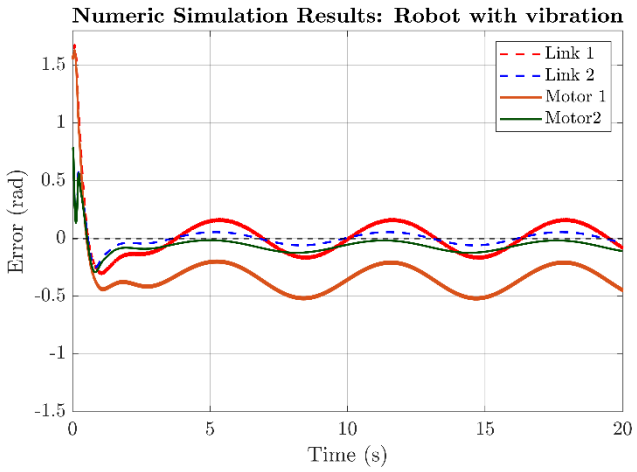

Fig. 8. Positioning error for LQR control with KI control; error for $\theta_1, \theta_2, \theta_3, \theta_4,$

Table 3. RMSE in case vibration excitation

Elements	K_LQR	K_LQR+KI
Link 1	0.342556	0.106650
Link 2	0.104594	0.036836
Motor 1	0.193504	0.338017
Motor 2	0.086688	0.063467

Vibration Rejection Analysis: As illustrated in **Fig. 7**, the standard LQR controller exhibits significant oscillating errors, struggling to suppress the link vibrations caused by the external excitation. The RMSE for Link 1 under standard LQR reaches a high value of 0.481502 rad.

Performance of Proposed LQR-KI: In contrast, **Fig. 8** shows that the LQR-KI controller significantly suppresses these oscillations. By utilizing the integral action within the augmented state-space framework, the RMSE for Link 1 is reduced by nearly 3 times, down to 0.1 rad. Similarly, the Link 2 RMSE improves from ~0.1 rad to ~0.03 rad.

Stability and accuracy: This superior disturbance rejection is achieved while maintaining the closed-loop poles strictly in the left-half plane, even at the worst-case configuration. Moreover, the error totally approximates 2% of the operational range (~0.03/1.54). This achievement is considered a "golden result" in the control field, especially for flexible-joint manipulators operating under high-frequency disturbances (100 rad/s).

4.3. Energy Efficiency Validation

In this scenario, we will make a simple rigid model by change stiffness and damping of joints into very high value.

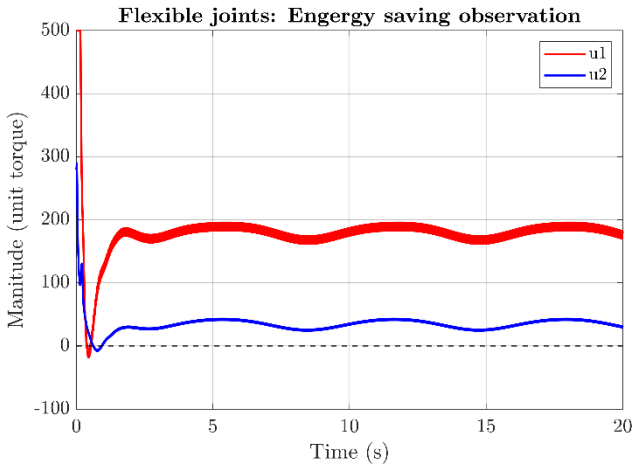

Fig. 9. Energy tracking in case flexible joints

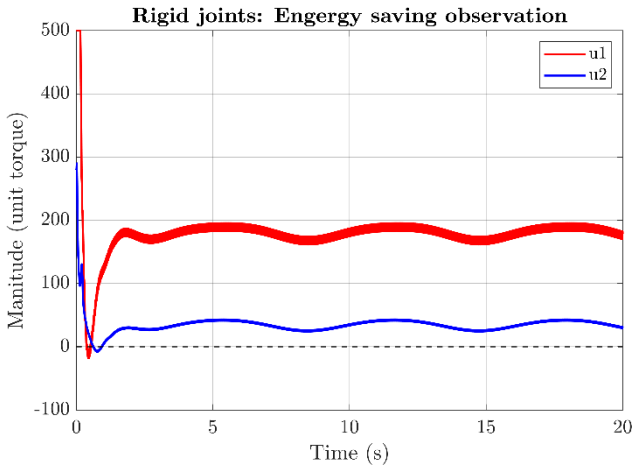

Fig. 10. Energy tracking in case rigid joints

Table 4. Energy consumption

Elements	Rigid joints (unit torque)	Float joints (unit torque)	Improve-ments (%)
Motor 1	192.06	180.89	5.81
Motor 2	49.52	38.07	23.12
Totally	241.58	218.96	9.36

The most significant finding of this study is the energy performance of the flexible-joint configuration under LQR-KI control. By exploiting the natural compliance of the joints and optimizing the control effort through the LQR cost function J, the system achieves an energy saving of approximately 9.36% compared to a conventional rigid-link system performing the same task. This confirms that the proposed model and controller is not only robust but also highly suitable for sustainable, battery-powered agricultural platforms.

5. Conclusion

The simulation results and stability analysis offer multi-dimensional perspectives on the effectiveness of the proposed LQR-KI strategy for flexible-joint manipulators in agricultural fields. This research has been demonstrated that:

Robust Precision: The LQR-KI scheme achieves a positioning error of less than 2%, effectively suppressing disturbances of 100 rad/s without complex feedforward terms.

Efficiency: The system achieves a verified 9.36% reduction in total energy consumption, supporting the feasibility of sustainable robotic platforms.

Guaranteed Stability: Eigenvalue analysis confirms global asymptotic stability, with closed-loop poles strategically placed to handle extreme field excitations.

6. Discussion on Energy and Mechanical Dynamics

The most significant finding is the 9.36% energy saving achieved by the flexible-joint configuration compared to the rigid-joint model. Fundamentally, a flexible joint acts as a natural low-pass filter. In the context of operation in an agricultural environment and affected by complex vibration disturbances, its physical compliance naturally absorbs high-frequency vibrations and reduces the impact of non-ideal excitations. While this mechanical property provides partial disturbance rejection, the robust LQR-KI controller contributes to enhancing the accuracy also the effeciency. By linearizing at the worst-case point and utilizing an augmented state-space, the controller eliminates the need for real-time re-linearization across the entire workspace. This fixed-gain approach significantly optimizes computational resources, making it highly suitable for low-power microcontrollers (e.g., STM32) that can operate without complex Gain Scheduling or Feedforward models. This synergy is crucial for agricultural environments, where battery-powered robots must maintain high accuracy under harsh conditions while minimizing power consumption.

Future work will focus on validating this control architecture using a Hardware-in-the-Loop (HIL) framework. In this approach, the refined 8th-order dynamics will be executed on a real-time simulator, while the hybrid control algorithm will be embedded into an industrial-grade microcontroller (e.g., STM32). This setup will allow for the evaluation of real-time constraints, such as sampling latency and signal quantization, ensuring the system's reliability for unpredictable agricultural field operations.

7. Appendix

The state-space matrix A, B as below:

Matrix A (standard):

$$\begin{bmatrix} 0 & 1 & 0 & 0 & 0 & 0 & 0 & 0 \\ -250 & -328.12 & 750 & 984.38 & 250 & 325 & -750 & -975 \\ 0 & 0 & 0 & 1 & 0 & 0 & 0 & 0 \\ 750 & 984.37 & -2500 & -3281.3 & -750 & -975 & 2500 & 3250 \\ 0 & 0 & 0 & 0 & 0 & 1 & 0 & 0 \\ 4\times10^5 & 5.2\times10^5 & 0 & 0 & -4\times10^5 & -5.2\times10^5 & 0 & 0 \\ 0 & 0 & 0 & 0 & 0 & 0 & 0 & 1 \\ 0 & 0 & 4\times10^5 & 5.2\times10^5 & 0 & 0 & -4\times10^5 & -5.2\times10^5 \end{bmatrix}$$

Matrix B (standard):

$$\begin{bmatrix} 0 & 0 \\ 0 & 0 \\ 0 & 0 \\ 0 & 0 \\ 0 & 0 \\ 800 & 0 \\ 0 & 0 \\ 0 & 800 \end{bmatrix}$$

Vector K_{LQR}:

$$\begin{bmatrix} 618.16 & 146.96 & -3.1828 & 38.051 & 0.54678 & 0.097415 & -0.18383 & -0.03772 \\ 106.62 & 39.694 & 192.96 & 17.256 & 0.025543 & -0.007544 & 0.28842 & 0.048803 \end{bmatrix}$$

Vector K_I:

$$\begin{bmatrix} 974.53 & -225.28 \\ 100.3 & 435.82 \end{bmatrix}$$

Matrix Q (extend):

$$\begin{bmatrix} 10^3 & 0 & 0 & 0 & 0 & 0 & 0 & 0 & 0 & 0 \\ 0 & 1 & 0 & 0 & 0 & 0 & 0 & 0 & 0 & 0 \\ 0 & 0 & 10^3 & 0 & 0 & 0 & 0 & 0 & 0 & 0 \\ 0 & 0 & 0 & 1 & 0 & 0 & 0 & 0 & 0 & 0 \\ 0 & 0 & 0 & 0 & 10^3 & 0 & 0 & 0 & 0 & 0 \\ 0 & 0 & 0 & 0 & 0 & 1 & 0 & 0 & 0 & 0 \\ 0 & 0 & 0 & 0 & 0 & 0 & 10^3 & 0 & 0 & 0 \\ 0 & 0 & 0 & 0 & 0 & 0 & 0 & 1 & 0 & 0 \\ 0 & 0 & 0 & 0 & 0 & 0 & 0 & 0 & 10^4 & 0 \\ 0 & 0 & 0 & 0 & 0 & 0 & 0 & 0 & 0 & 10^4 \end{bmatrix}$$

Matrix R:

$$\begin{bmatrix} 0.01 & 0 \\ 0 & 0.05 \end{bmatrix}$$

Table 5. Total Poles of the closed-loop system

Poles	The located position
1	*-0.76922*
2	*-0.76924*
3	*-2.3476 + 3.0021i*
4	*-2.3476 - 3.0021i*
5	*-2.73*
6	*-3.2036*
7	*-17.8*
8	*-49.103*
9	*-5.2011e+05*
10	*-5.2358e+05*

References

[1] TUSSET, Angelo M., et al. Positioning Control of Robotic Manipulators Subject to Excitation from Non-Ideal Sources. *Robotics*, 2023, 12.2: 51.

[2] ALAM, Waqar, et al. Control of flexible joint robotic manipulator: Design and prototyping. In: 2018 International Conference on Electrical Engineering (ICEE). IEEE, 2018.

[3] Rad, S.A., Tamizi, M.G., Mirfakhar, A., Masouleh, M.T., Kalhor, A.: Control of a two-DOF parallel robot with unknown parameters using a novel robust adaptive approach. ISA Trans. 117, 70–84 (2021)

[4] PENA, Alejandro, et al. An evolutionary intelligent control system for a flexible joints robot. Applied Soft Computing, 2023

[5] MA, Hui, et al. Adaptive prescribed performance control of a flexible-joint robotic manipulator with dynamic uncertainties. IEEE Transactions on Cybernetics, 2021

[6] RAMÍREZ-NERIA, Mario, et al. On the tracking of fast trajectories of a 3DOF torsional plant: A flatness based ADRC approach. Asian Journal of Control, 2021

[7] LIU, Xiangchen; WANG, Minghai; WANG, Yihan. Improved vibration suppression strategy of fuzzy PI servo control for dual flexible system with flexible joints. Mathematics, 2023

[8] LI, Rong, et al. Robust Model Predictive Control for Two-DOF Flexible-Joint Manipulator System. Mathematics, 2023

[9] Mattioni, A.; Wu, Y.; Le Gorrec, Y. Infinite dimensional model of a double flexible-link manipulator: The Port-Hamiltonian approach. Appl. Math. Model. 2020

[10] Kunming, Z.; Youmin, H.; Wenyong, Y. A novel parallel recursive dynamics modeling method for robot with flexible bar-groups. Appl. Math. Model. 2020

[11] AMATO, Gerardo; D'AMATO, Roberto; RUGGIERO, Alessandro. Adaptive rejection of a sinusoidal disturbance with unknown frequency in a flexible rotor with lubricated journal bearings. Mathematics, 2022, 10.10: 1703.

[12] XIONG, Genliang; SHI, Jingxin; CHEN, Haichu. Cascaded Control of Flexible-Joint Robots Based on Sliding-Mode Estimator Approach. Journal of Robotics, 2020, 2020.1: 8861847.

[13] YANG, Siyang, et al. An optimal fuzzy-theoretic setting of adaptive robust control design for a lower limb exoskeleton robot system. Mechanical Systems and Signal Processing, 2020

[14] NOHOOJI, Hamed Rahimi. Constrained neural adaptive PID control for robot manipulators. Journal of the Franklin Institute, 2020

[15] PEZZATO, Corrado; FERRARI, Riccardo; CORBATO, Carlos Hernández. A novel adaptive controller for robot manipulators based on active inference. IEEE Robotics and Automation Letters, 2020,

[16] WANG, Xingyu, et al. A two-layer trajectory tracking control scheme of manipulator based on ELM-SMC for autonomous robotic vehicle. IEEE Transactions on Automation Science and Engineering, 2023

[17] ALI, Mohammed; MIRINEJAD, Hossein. Robust tracking control of flexible manipulators using hybrid backstepping/nonlinear reduced-order active disturbance rejection control. ISA transactions, 2024

[18] ASGHAR, Arafat, et al. Performance comparison of structured H∞ based looptune and LQR for a 4-DOF robotic manipulator. Plos one, 2022

[19] LIN, Jiafeng, et al. A Fuzzy Logic Approach to Power System Security with Non-Ideal Electric Vehicle Battery Models in Vehicle-to-Grid Systems. IEEE Internet of Things Journal, 2025.

[20] Bilal, H.; Yin, B.; Aslam, M.S.; Anjum, Z.; Rohra, A.; Wang, Y. A practical study of active disturbance rejection control for rotary flexible joint robot manipulator. Soft Comput. 2023

[21] Li, Z.; Li, P.; Ye, Y.; Liu, X. A modified active disturbance rejection control method for the compliance control of the flexible joint robots. In Proceedings of the 2022 IEEE International Conference on Robotics and Biomimetics, ROBIO 2022

[22] URREA, Claudio; KERN, John. Recent Advances and Challenges in Industrial Robotics: A Systematic Review of Technological Trends and Emerging Applications. Processes, 2025, 13.3: 832.

[23] KESHVARPARAST, Ali, et al. Collaborative robots in manufacturing and assembly systems: literature review and future research agenda. Journal of Intelligent Manufacturing, 2024, 35.5: 2065-2118.

[24] SUN, Yufang. Automatic vibration control method for grasping end of flexible joint robot. Journal of Vibroengineering, 2023, 25.8: 1502-1515.

[25] ARENTS, Janis; GREITANS, Modris. Smart industrial robot control trends, challenges and opportunities within manufacturing. Applied Sciences, 2022, 12.2: 937.

[26] JU, Jinyong, et al. Vibration suppression of a flexible-joint robot based on parameter identification and fuzzy PID control. Algorithms, 2018, 11.11: 189.

[27] TUSSET, A. M., et al. A hybrid PID-LQR control applied in positioning control of robotic manipulators subject to excitation from non-ideal sources. In: Nonlinear Vibrations Excited by Limited Power Sources. Cham: Springer International Publishing, 2022.